Chapter 10

Mechanical Properties of Porous Ceramics

Vânia Regina Salvini, Victor C. Pandolfelli and Dirceu Spinelli

Additional information is available at the end of the chapter

http://dx.doi.org/10.5772/intechopen.71612

Abstract

It is widely known that increasing interest in porous ceramics is due to their special properties, which comprise high volumetric porosity (up to 90%) with open or closed pores, and a broad range of pore sizes (micropores: d < 2 nm; mesopores: 50 nm > d > 2 nm and macropores: d > 50 nm). These properties have many uses comprehending macroscaled devices, mesoscaled materials and microscaled pieces. During their usage, these materials are usually submitted to thermal and/or mechanical loading stresses. Therefore, it is a premise to understand how these porous structures behave under thermomechanical stresses to design materials that show adequate properties for the required application. In this context, the aim of this chapter is to review the mechanical properties of macroporous ceramics.

Keywords: porous ceramics, foams, mechanical properties, elastic modulus, fracture energy

1. Introduction

It is widely known that increasing interest in porous ceramics is due to their special properties, which comprise high volumetric porosity (up to 90%) with open and interconnected or closed and isolated pores, and a broad range of pore sizes (micropores: d < 2 nm; mesopores: 50 nm > d > 2 nm and macropores: d > 50 nm). These properties have many uses comprehending macroscaled devices (filters for liquid metals [1, 2], thermal insulating refractories [3, 4], bioceramics for bone regeneration [5–7], filters for water treatment [8], acoustic insulating tiles [9]),

mesoscaled materials (membranes for catalysis [10], drug release substrates [11, 12]) and microscaled pieces (e.g., multifunctional materials where gravimetric properties are critical as batteries [13] and electronic sensors [14]).

During their usage, these materials are usually submitted to thermal and/or mechanical loading stresses. Therefore, it is a premise to understand how these porous structures behave under thermomechanical stresses to design materials that show adequate properties for the required application.

Despite the importance of porosity for application of these materials, there is not a general consensus about the dependence of mechanical properties on porosity parameters. In other words, the real data of the mechanical properties of these materials indicate that their mechanical behavior depends on more than just porosity of the materials.

Since its introduction to the ceramic community in the 1970s, the area of fracture mechanics has made significant contributions to improving ceramics. As an example, the combination of fracture toughness, fracture statistics and fractography has made it possible to identify critical flaws in material and, consequently develop better and reliable advanced ceramics. In addition, the contribution of fracture mechanics was fundamental in understanding the fracture process in brittle materials.

Recognizing that the area behind a crack was responsible for the increase in the R-curve in ceramics was particularly relevant. One issue concerning the uses of brittle ceramics is associated with the statistical and size-dependence of their fracture properties, which can make reliable prediction, a difficult task. Two other problems are the absence of design methodology for brittle ceramics and the high costs of producing the ceramic components [15].

Nowadays, the ceramic community is witnessing a "boom" of nature inspired materials using hierarchical structures that should have the same behavior or qualities as the natural ones. Various papers [16–20] in the literature show beautiful structures of natural materials and their mimicked copies by researchers. The capacity of a human being's observation, also a characteristic controlled by nature, has been the driving force to imitate natural hierarchical structures and their qualities.

In this context, the aim of this chapter is to review the mechanical properties of macroporous ceramics. The following issues are of particular interest to this chapter:

1. Which microstructural parameters affect the mechanical strength of the porous ceramic material besides its porosity?
2. To what extent do the pores affect the fracture toughness of the porous ceramic material? Does it make sense to measure the fracture toughness of porous material knowing that the stress intensity factor at the notch tip is decreased by the presence of surrounding pores? Or, instead of this, would the total fracture energy be a more realistic measure?
3. What is the elastic modulus behavior of porous ceramics as a function of temperature?

All these questions need to be considered in order to advance not only the processing of porous ceramic materials but also to design their structures for specific applications.

http://dx.doi.org/10.5772/intechopen.71612

2. Influence of microstructural parameters on the mechanical strength of porous ceramic materials

The objective here is not to carry out an extensive revision of the fracture of brittle porous materials, but to present results which serve as a basis to the authors´ proposal in this chapter.

First of all, fracture of porous ceramics is better described by the quasi-brittle behavior as their ultimate fracture is triggered by many local events (different from essentially brittle behavior of glass ceramics), yet they are not preceded by highly dissipative processes associated with plastic deformation and strain hardening (as observed in ductile metals) [21]. Quasi-brittle fracture behavior is also observed in rocks, bones and ceramic composites.

As mentioned earlier, the real data of the mechanical properties of porous materials indicate that their mechanical behavior depends on more than just porosity of the materials.

Questions have been raised about the models proposed by Gibson and Ashby (GA) [22, 23], which indicate that the relative strength of a porous material is a function of its relative density as follows:

$$\frac{\sigma}{\sigma_s} = C\left(\frac{\rho}{\rho_s}\right)^m \tag{1}$$

where σ and ρ are, respectively, the fracture strength and the density of porous material; σ_S and ρ_S are the fracture strength and the density of solid material, respectively; C is a dimensionless constant and the exponent m depends on the pore morphology (m = 3/2 for open pores or m = 2 for closed ones). The Gibson and Ashby (GA) models are based on the bending or buckling of cell edges.

Figure 1 shows the relative strength predicted by the Gibson and Ashby models plotted together with experimental data of porous ceramics from different researchers. It can be seen a disagreement between the theoretical curves of GA models and the experimental results.

Colombo et al. [24] attributed microstructural factors for the lack of fitting data to the Gibson and Ashby models, as shown in **Figure 1**, as they do not consider the distribution of pore sizes, neither have mixed pores (open and closed) nor flaws in the pore wall (struts).

Seeber et al. [25] also noted that the drop in mechanical properties of foamed ceramics was disproportionately greater than what was to be expected solely from increasing the porosity. These authors suggested this behavior must be an influence of the pore size or the strut thickness, as reported by Brezny and Green [26] in a previous paper.

Nevertheless, Salvini et al. [27] suggested that a parameter which expresses the processing method to produce the porous structure should be considered by the mechanical models. For instance, porous ceramics with similar porosity and density ranges can be produced using different ceramic methods such as sacrificial fugitives, replica templates and directing foaming. However, each method provides a different number of struts (ligaments) of distinct solid particle packing, which influences the final mechanical behavior of the material.

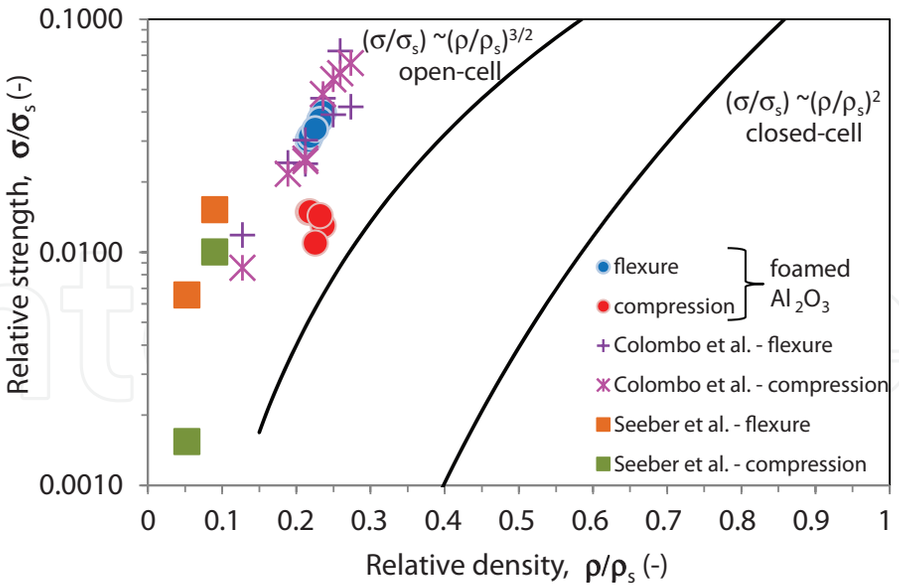

Figure 1. Plot of relative strength as a function of relative porosity for Gibson and Ashby (GA) models [22, 23] and for experimental data obtained by Salvini et al. [27], Colombo et al. [24] and Seeber et al. [25].

In this context, Lichtner et al. [28] produced porous ceramics of same porosity but different pore arrangement using the freeze casting and the slip casting processing methods. They have noted a strong influence of processing on the mechanical properties, and attributed to the differences of orientation and connectivity of macropores.

Brezny et al. [29] also reported that strength of the struts is an important parameter controlling the properties of porous ceramics. According to them, an increase in the strut strength would be expected as a result of the reduced probability of finding a critical flaw in a smaller volume of material as predicted by Weibull, the weakest link hypothesis for strength variability.

Additionally, Genet et al. [21] pointed out that the Gibson and Ashby's approach cannot directly deal with the statistical and size-dependent aspects of fracture.

In 1996, Rice [30] had already drawn attention to this debate considering some problems with micromechanics-based models. The first concern mentioned by Rice was the assumption that porous bodies are represented by packing of hollow spherical particles of an infinite range of sizes. Then, it is assumed the application of a hydrostatic pressure is uniformly distributed in all particles so the resulting strain response can be calculated. Moreover, a common approach to improving the agreement between these models is to let some parameter, for example, the Poisson ratio, depends on the porosity, that is, using it as an adjustable parameter. Another concern is that these models assume that porosity will remain fixed during applications.

Then, Rice has proposed that the mechanical strength of porous ceramics should depend not only on the relative density but also on the minimum solid area fraction, as depicted in **Figure 2**. That is because the solid area is required for transmission of mechanical stresses and thermal and electrical fluxes. This concept is schematically presented in **Figure 3**.

As can be seen in **Figure 2**, each specific model has the following three characteristics: (1) a nearly linear slope of the first half to three-quarters of the porosity range, (2) the approximate

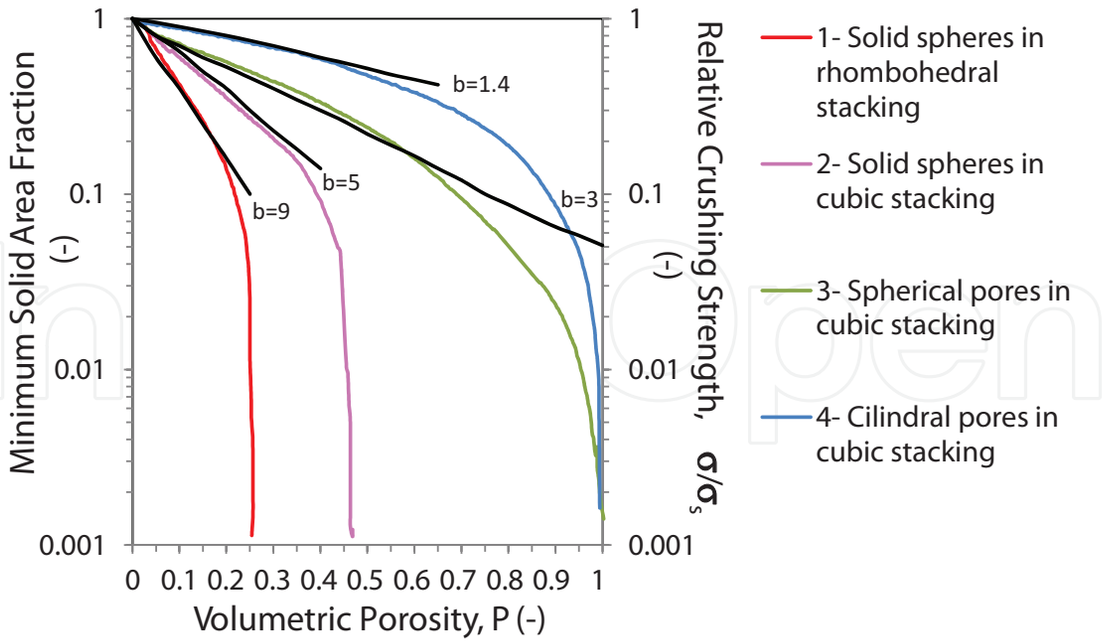

Figure 2. Models from the literature showing the effects of the minimum solid area and porosity on the strength for three basic sphere stackings (cubic, rhombohedral and a mixture of them) and for cylindrical or spherical pores, as well as their mixture, in cubic stacking. The nearly linear portion of curves is represented by the semilogarithmic expression $\sigma = \sigma_S\, e^{-bP}$, with b values ranging from 1 to 3 for stacked pores and from 3 to 9 for stacked particles [30].

porosity value where properties start to be damaged more significantly than the linear slope and (3) the critical porosity P_C where properties go to zero.

However, as pointed out by Rice, these characteristics are useful in distinguishing the basic porosity character of each stacking model, but their utility varies. For instance, P_C values can be accurately defined theoretically, but obtaining reliable experimental data can be a difficult task.

Moreover, the approximated linear slopes are unique for the basic stacking models, and they have been the most widely available factor for polycrystalline materials. However, as clearly shown in **Figure 2**, they can be applied for the restricted porosity range only.

More recently, Bruno et al. [31] reviewed micromechanics aiming the development of microstructure-property relations for porous microcracked ceramics. They focused on specific issues for porous ceramics as the nonlinear stress–strain behavior and the thermal-induced microcracking.

Zheng et al. [32] considered that the fracture strength of brittle porous material is nonlinear and, therefore, there is a percolation failure phenomenon at the fracture of these materials. Therefore, their model considers the porosity (P) and the elastic percolation (ϕ), which depends on the Poisson's ratio of material, as shown:

$$\frac{\sigma}{\sigma_S} = \left[\left(\frac{\phi - P}{\phi}\right)^{1+\nu} \cdot \left(1 - \phi^{2/3}\right)\right]^{1/2} \tag{2}$$

$$\phi = 1 - \left[\frac{1+\upsilon}{3(1-\upsilon)}\right] = \frac{2(1-2\upsilon)}{3(1-\upsilon)} \tag{3}$$

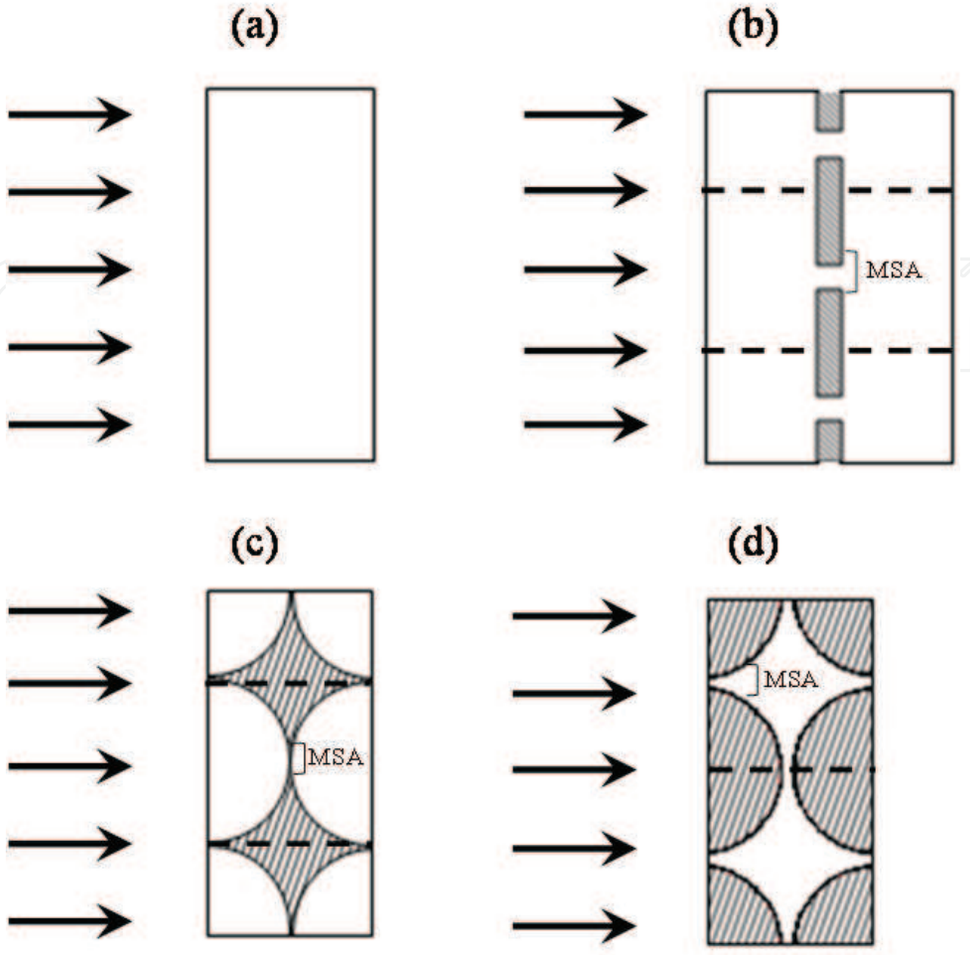

Figure 3. Diagram of the minimum solid area concept. (a) Cross section of a dense material showing the uniform transmission among layers normal to a uniform mechanical stress or conductive flux. (b) Cross section of material showing some layers were removed, leaving only small continuous areas (MSA) for transmission of stress or flux. (c) Cross section of stacked particles and (d) cross section of stacked pores where again the minimum areas of solid will control the transmission of stress or flux normal to the plane of slab [30].

where ν is the scaling exponent for tridimensional solids and υ is the Poisson ratio of materials. In general, for ceramics $\upsilon = 0.2$ and $\phi = 0.5$, for metals $\upsilon = 0.3$ and $\phi = 0.38$, and for polymers $\upsilon = 0.33$ and $\phi = 0.338$. Zheng et al. [32] validated the proposed model for polymers using different porosities and experimentally measured them using the three-point-bending strength test.

In order to check the validity of Zheng's model, Salvini et al. [27] considered the fracture flexure strength data of foamed Al_2O_3 with porosity of 76%. Nevertheless, the results must be interpreted with caution, as Zheng's model overestimated the flexure strength indicating values around 25 MPa, while the average experimental value obtained by Salvini et al. [27] was 10 MPa.

Regarding the failure patterns, Genet et al. [21] investigated the fracture mechanism across scales of porous ceramic scaffold applying a computational method. **Figure 4** shows the

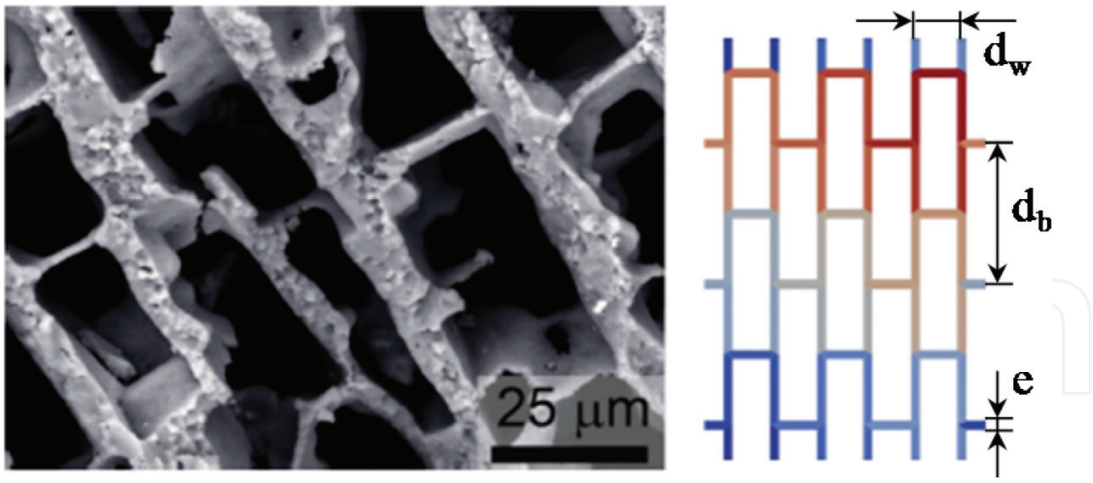

Figure 4. SEM image of a porous ceramic scaffold made by the freeze casting method and its associated idealized geometry, which consists of walls connected by bridges positioned in staggered rows. The geometrical parameters are as follows: The distance between the walls, d_w (d_w = 25 μm), the distance between the bridges, d_b (d_b = 75 μm), and the thickness of the walls and bridges, e (e = 5 μm). A microcell is defined by r × r RVEs (representative volume elements) [21].

scanning electron microscopy (SEM) image of the porous scaffold made by freeze casting and the respective idealized geometry.

Genet et al. [21] found that for very small-sized samples (r = 1 × 1 RVEs), the fracture is brittle and is triggered by the first strut to break. For intermediate-sized samples (r = 5 × 5 RVEs), however, the fracture is controlled by the percolation of several strut breaks, and is mainly governed by the stress redistribution after each break. For large-sized samples (r = 256 × 256 RVEs), they found that the failure process appears to be different, and it is divided into two stages.

The initial stage consists of a widespread development of damage due to the failure of the weakest local defects. But, the stress redistribution caused by these failures is not high enough to make the neighboring cells break or initiate a macrocrack. Instead, a critical defect is activated, rapidly leading to the development of a macrocrack, which leads to the final fracture of the material. Then, the "fatal" macrocrack in large samples does not result from the percolation of previously damaged cells/pores.

Nevertheless, there are some limitations in this study. Firstly, the computational analyses were based on the assumption that porous scaffold material presents isotropic Young's modulus and Poisson's ratio. Another limitation of this study is that the fracture behavior was evaluated under one loading direction only (pure traction).

Although using high resolution tomography to evaluate the failure behavior of porous ceramics, Berek et al. [33] and Petit et al. [34] independently identified the same fracture pattern as proposed by Genet et al. [21]. Recently, Cui et al. [35] also found the nonlinear mechanical behavior due to the accumulation of local damage in porous ceramics.

In different works, Brezny et al. [26] and Morgan et al. [36] studied the effect of the cell size of glassy porous ceramics on their mechanical properties. Both authors reported the mechanical

strength of cellular ceramics increased with decreasing cell sizes. They attributed this behavior to a reduction in the critical flaw size as well as the increasing strut strength in smaller cell sizes.

Meanwhile, Deng et al. [37] investigated the reinforcement mechanisms of fine- and coarse-grain porous SiC and found that the crack-tip blunting mechanism in porous material, as shown in **Figure 5**, increases the fracture toughness of the material. They also noted that the larger the pore size in front of the crack, the more the fracture toughness of the porous ceramic is relative to its fracture strength. However, a detailed discussion about the fracture toughness of porous ceramics is provided in the next section.

Based on the *Stress Concentration Design Factors,* Peterson [38], Deng et al. [37] and Rice [39] attributed this behavior to the interactions between pores. Rice [39] combined Peterson's data in **Figure 6** to show that the stress concentration diminishes significantly as the pores become closer and the pore interactions begin to no longer be negligible when the center-to-center distance between them is around two times their diameter. Specifically, for the case where pores touch each other, in porosity of 78%, **Figure 6** shows that the stress concentrations become very low.

In reviewing the literature about mechanical properties of porous ceramics, it can be summarized which parameters affect, and to what extent, the strength of this class of ceramic materials.

On the one hand, there are researches considering the pores as the stress concentrations for the material fracture. Therefore, these researches consider the mechanical properties of porous ceramics depend only on the relative porosity.

On the other hand, other researches have considered the interactions among pores as low as 10% of porosity, which reduce the stress concentration factor for fracture. Then, they take into account the mechanical properties of porous ceramics depend on pores-stress interactions.

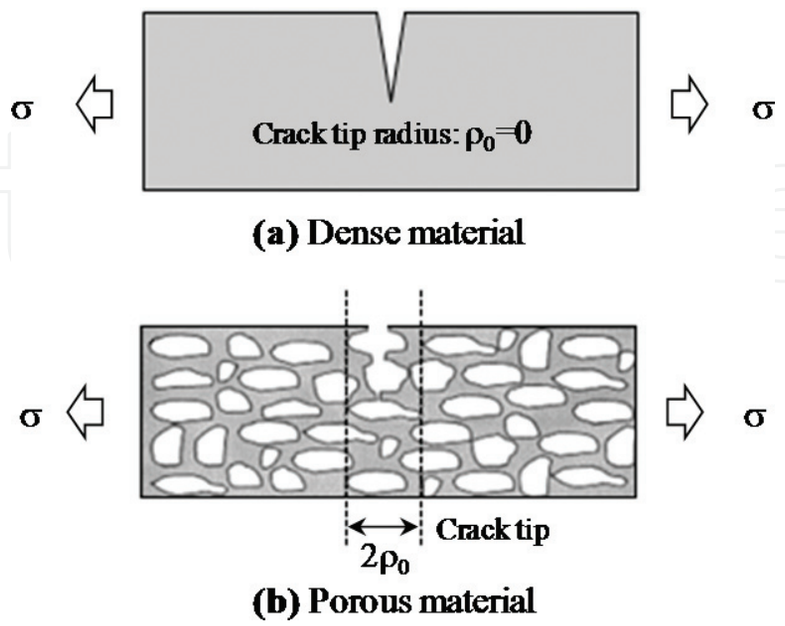

Figure 5. Representation of a crack propagated in (a) dense ceramic with a sharp crack-tip and in (b) porous ceramic where the crack-tip becomes blunt [37].

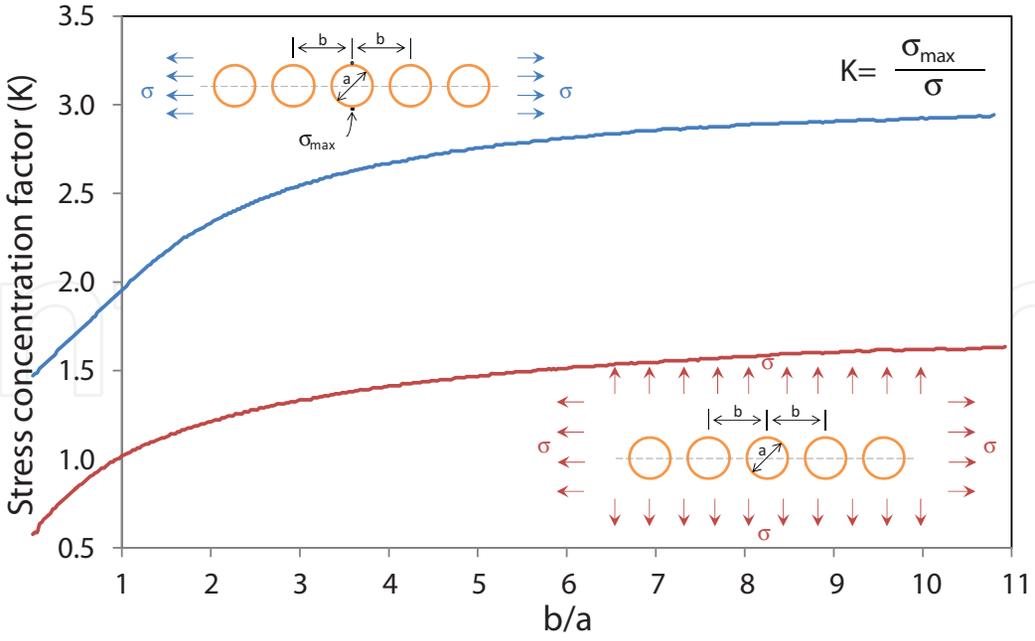

Figure 6. Stress concentration factors for a chain of holes in either uniaxial or in biaxial tension [38].

Regarding pore-stress interactions, there is strong evidence in the literature [40–42] concerning the mechanical behavior of human bones (also a quasi-brittle material) to support the hypothesis that microstructural changes in material may be essential in controlling its strength. The considered microstructural parameters are the porosity, size of pores, number and thickness of struts connecting the pores.

In human bodies, the mechanical properties of natural bone change with their biological location because the crystallinity, porosity and composition of bone adjust to the biological and biomechanical environment. For these materials, the bone volume fraction (bone volume BV/total volume TV) is given as a function of the thickness-to-length ratio, that is, t/ℓ, as shown in the following expression:

$$\frac{BV}{TV} = \frac{33\,\pi}{80\,\sqrt{2}}\left(\frac{t}{\ell}\right)^2 \tag{4}$$

Changes in the microstructure of the vertebral trabecular bone with aging have been quantified by histomorphometric analysis and also simulated by a computer using finite element software in two-dimensional (2D) [41] and three-dimensional (3D) [42] microstructural models. The microstructural changes of the bone include reductions in the trabecular thickness (t) and number (N), as shown in **Figure 7**. Both changes are strongly correlated with reductions in bone volume fraction and represent the two fundamental changes in microstructure associated with reduced bone volume [40–42].

Silva et al. [41] showed, using a 2D model, that once significant numbers of trabeculae (ligaments) are lost, it is impossible to recover the original mechanical properties of bone merely by increasing the trabeculae thickness, indicating the importance of the trabeculae number (N) and the integrity of its microstructure.

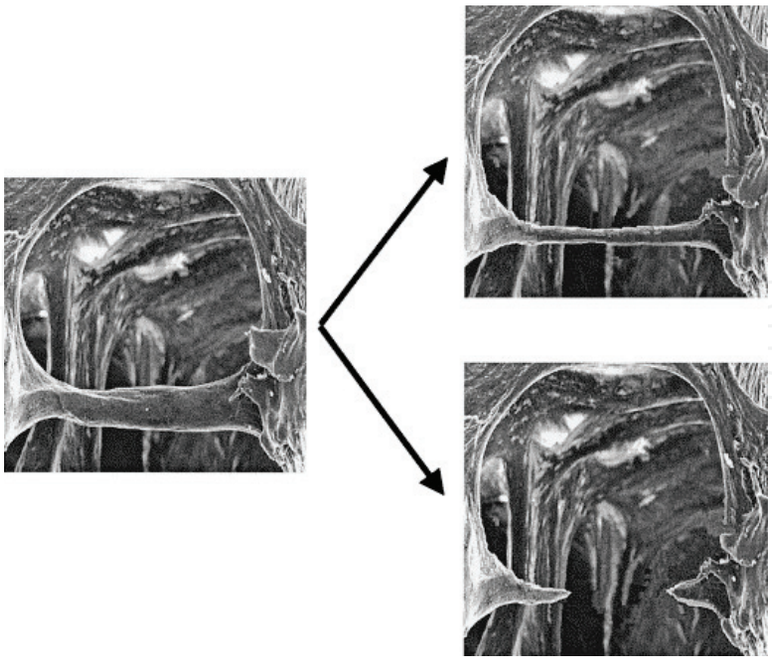

Figure 7. Simulated images of the trabecular bone showing two types of bone loss. Top right: thinning of trabeculae (ligaments) and bottom right: loss of trabeculae [42].

Considering the different types of trabeculae microstructures in 3D (rod-like and plate-like as shown in **Figure 8**), Guo et al. [42] quantified the changes in the Young's modulus and mechanical strength due to the trabecular bone loss. They considered the arrangement of tetrakaidecahedral cells as a 3D model for trabecular bones as shown in **Figure 8**. The cells filled in the 3D space were connected by either all beams (rod-like model) or all plates (plate-like model).

For each case of trabeculae loss simulation, the apparent Young's modulus and mechanical strength were normalized by the values of corresponding initial intact models (E_0 = 15 GPa, σ_0 = 100 MPa, Poisson's ratio of 0.3 at $t/\ell = 0.1$).

Quantitative relationships between mechanical strength and bone volume fraction (BV/TV) for the two types of bone loss in rod-like and plate-like models are presented in **Table 1** and **Figure 9**.

In the case of the rod-like model (**Figure 9a**), the loss of oblique trabeculae showed that the reductions in mechanical strength were more severe when the trabeculae thickness was reduced. In addition, after 13% loss of bone volume fraction (BV/TV), there was a dramatic reduction in strength due to the loss of the horizontal trabeculae.

For the plate-like model (**Figure 9b**), the reductions in mechanical strength due to trabeculae loss were also much more significant than those due to uniform trabeculae thinning. The quantitative relationships between the mechanical strength and bone volume fraction (BV/TV) due to trabeculae loss were dramatically different from those for trabeculae thinning (see **Table 1**).

These results suggest the importance of microstructural integrity such as the connectivity of the trabeculae bone architecture to maintain the mechanical integrity of bones. Besides, the extent of reduction in the mechanical properties due to trabeculae loss depends on the types of microstructures in the bone.

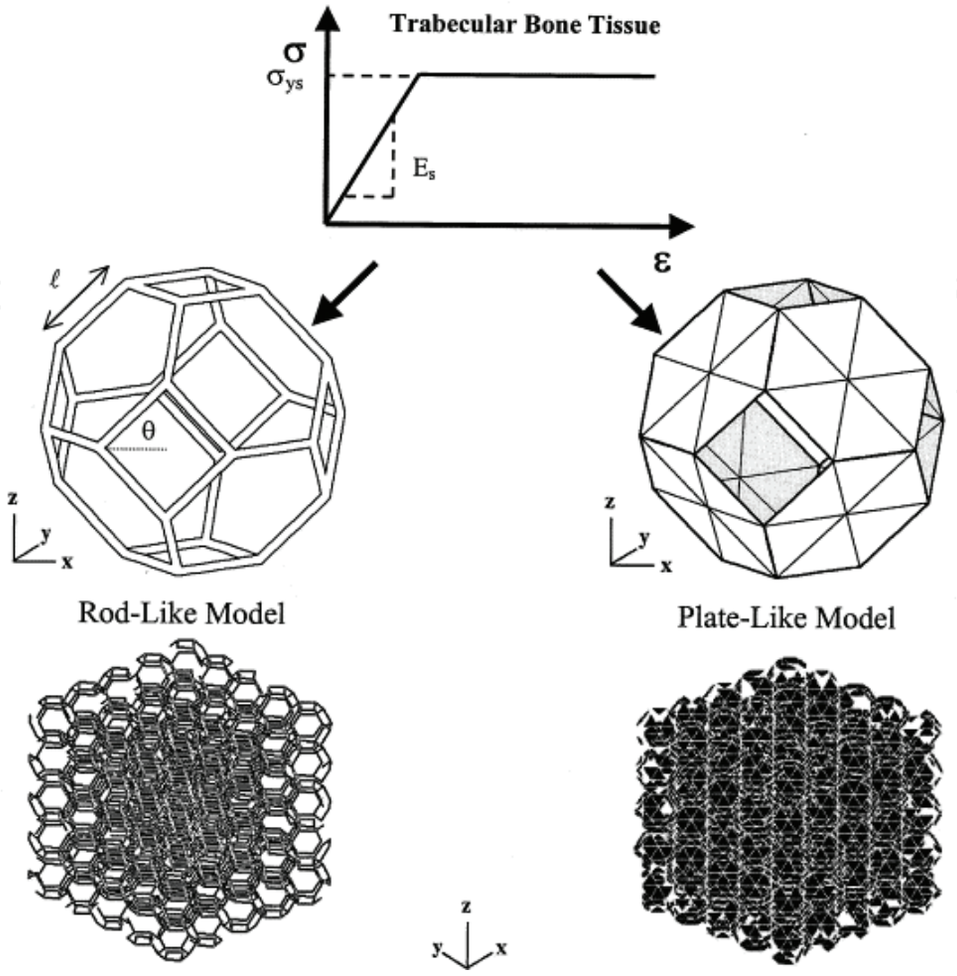

Figure 8. The 3D microstructural model of the trabecular bone. Each single cell has an edge of equal length, ℓ. θ = 45° for an isotropic structure. The entire model consists of arrays of 5 × 5 × 5 cells [42].

Model type	Bone loss type	Mechanical strength
Rod-like	Trabeculae thinning	$\frac{\sigma^*}{\sigma_0} = 0.592\ \left(\frac{BV}{TV}\right)^{1.60}$, $r^2 = 0.99$
Plate-like	Trabeculae thinning	$\frac{\sigma^*}{\sigma_0} = 0.378\ \left(\frac{BV}{TV}\right)^{1.10}$, $r^2 = 0.99$
Rod-like	Horizontal trabeculae loss	$\frac{\sigma^*}{\sigma_0} = 1.65x10^3\ \left(\frac{BV}{TV}\right)^{3.27}$, $r^2 = 0.85$
	Oblique trabeculae loss	$\frac{\sigma^*}{\sigma_0} = 4.69x10^{10}\ \left(\frac{BV}{TV}\right)^{6.94}$, $r^2 = 0.99$
Plate-like	Trabeculae loss	$\frac{\sigma^*}{\sigma_0} = 1.36x10^2\ \left(\frac{BV}{TV}\right)^{3.36}$, $r^2 = 0.99$

Table 1 Relationships between mechanical strength and bone volume (BV/TV) for two types of bone loss in rod-like and plate-like models [42].

Thus, for the natural bones, the number of ligaments (trabeculae) between pores appears to be much more effective to increase the strength of the material in comparison to the ligament thickness.

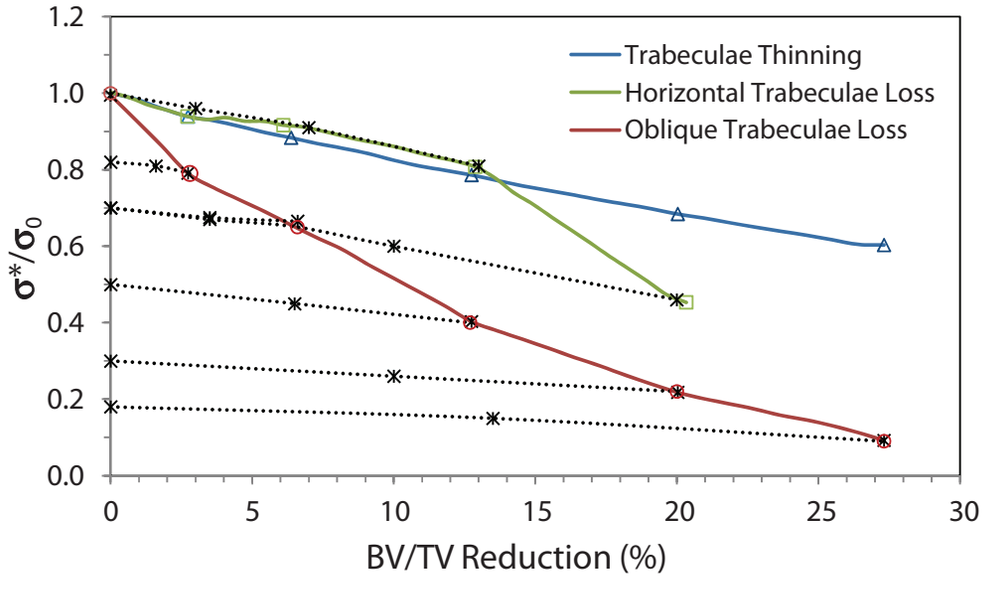

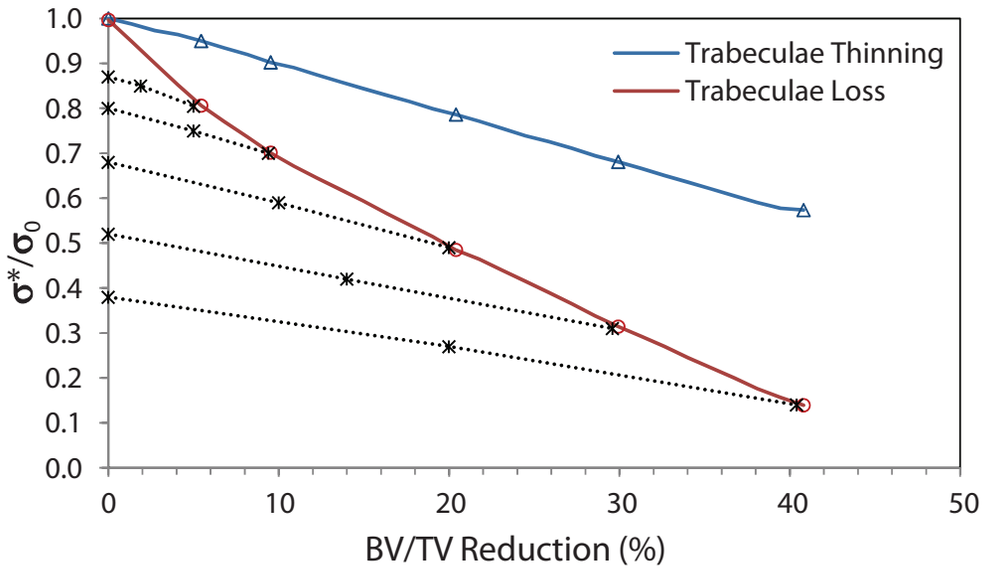

Figure 9. Reduction in the strength (a) of the rod-like model and (b) plate-like model due to bone loss (trabeculae thinning and trabeculae loss) represented by solid lines. Strength recovery by subsequent treatment with thickening trabeculae is represented by the dotted lines [42].

Lichtner et al. [28] also found the mechanical properties of freeze casting porous ceramics that are controlled by the connectivity of pore walls.

Similar mechanical behavior was reported by Salvini [43] for SiC ceramic filters of the same porosity (85%) but with different pores per inch (ppi), number of struts and average pore sizes (**Figure 10**). It can be seen in **Figure 10** that there is a rise in the number of connecting struts when the pore per inch (ppi) increases.

http://dx.doi.org/10.5772/intechopen.71612

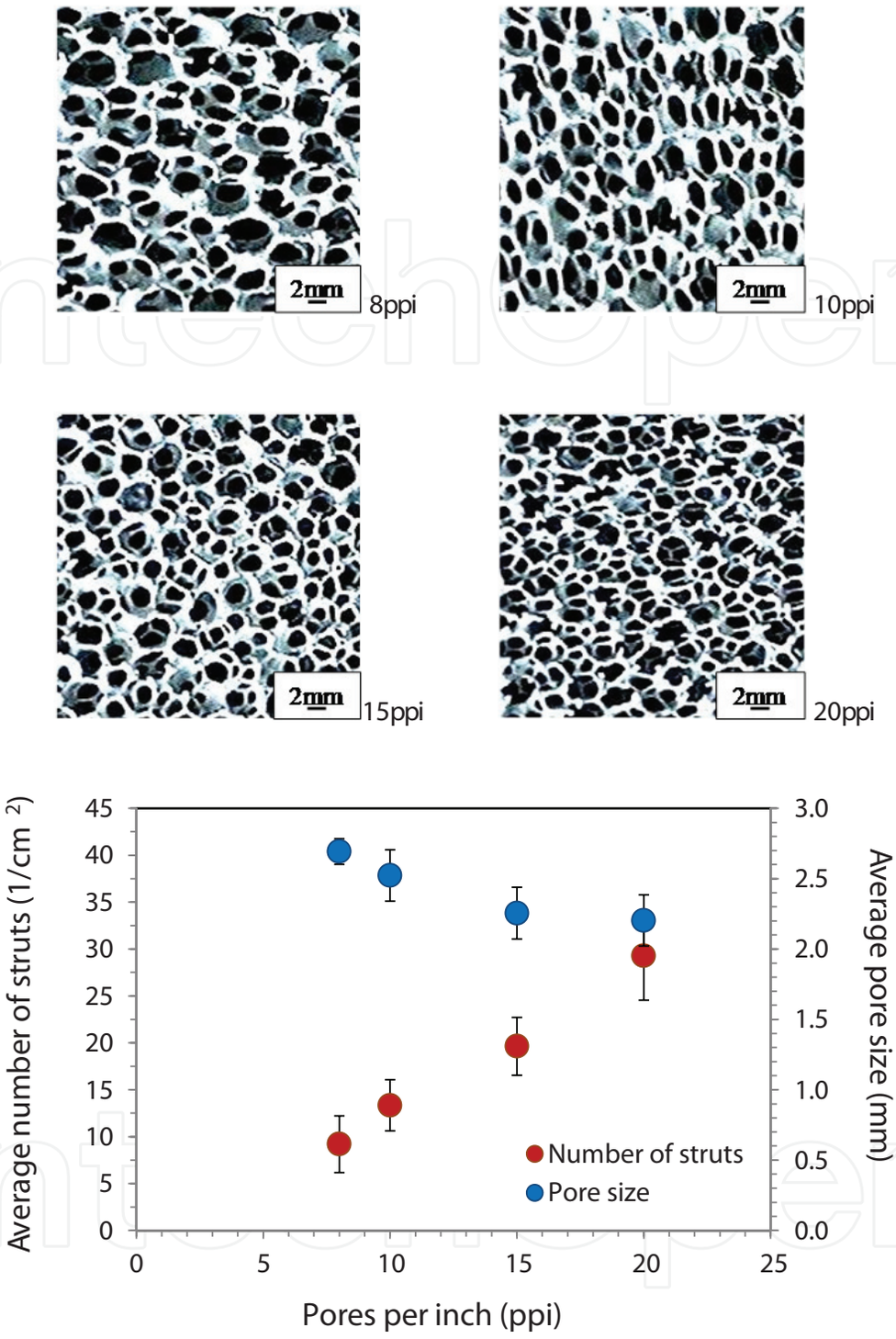

Figure 10. Physical characteristics of SiC ceramic filters of the same porosity (85%) but with different pores per inch (ppi) [43].

Moreover, differences were found between the strut number and pore size tendencies as a function of pores per inch (ppi). Interestingly, the number of connecting struts is sensitive to the variation of the number of pores (ppi).

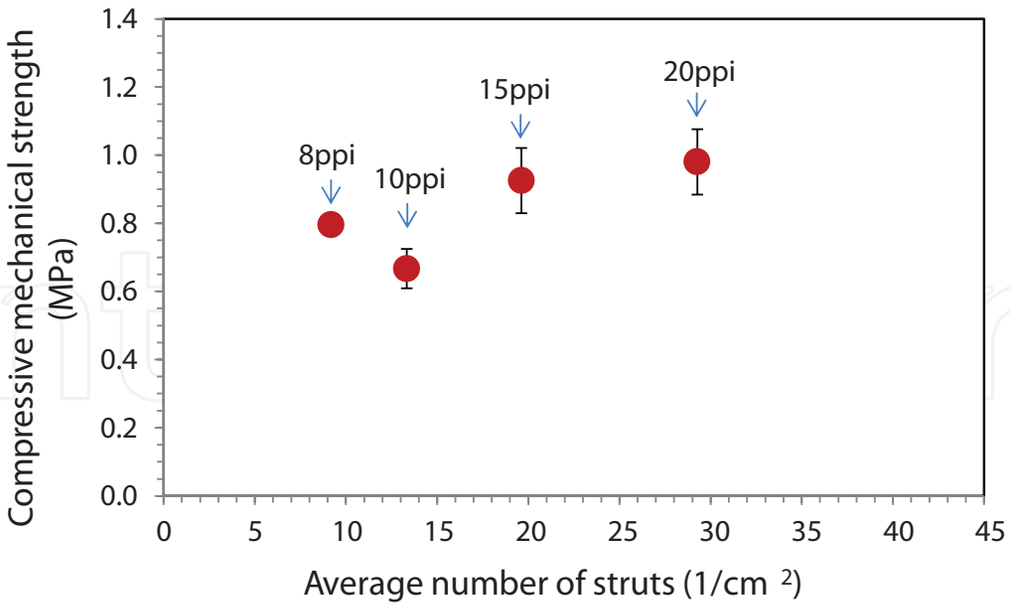

Figure 11. Compressive mechanical strength of SiC ceramic filters of the same porosity level (85%), but with different average pore sizes and number of connecting struts [43].

The high number of connecting struts in the SiC filters of high pores per inch (ppi) is more probably contributed to their increasing mechanical strength, as depicted in **Figure 11**.

A possible explanation for this mechanical behavior in SiC ceramic filters, as well as in trabeculae bones, might be the diminution of the stress concentration factor due to the stress-pore interactions, which is very low for porosity higher than 78% (see **Figure 6**).

One of the more significant findings to emerge from this section is that, in addition to the porosity of porous ceramics, the number of connecting struts between the cells/pores in the microstructure plays a fundamental role in their mechanical strength behavior.

3. Fracture toughness of porous ceramics

A requirement for almost structural materials is that they are both strong and tough yet invariably, in most materials, the properties of strength and toughness are mutually exclusive [44]. Whereas strength of material is a stress indicating its resistance to nonrecovery deformation, toughness is the resistance of material to the propagation of a crack and, then is measured as the energy required to cause fracture.

The ability of material to experience limited plastic deformation is a critical aspect to toughness, as this characteristic enables the local dissipation of high stress that would otherwise cause the fracture of material. That is the reason why the design methodology based on yield strength of materials is a common practice in the engineering [45].

Concerning fracture toughness (K_{IC}) methods for brittle ceramics, there are several tests which have been used such as the precrack by indentation, the single-edge notch beam (SENB) and

Chevron notch (CV) methods, which are the most common tests. All methods involve application of force to a beam test specimen in three or four point flexures.

Each method has limitations and the major problem is that significant effects due to the microstructure, for example, grain size and porosity, are not addressed in the continuum mechanics basis of these tests.

As proposed by Rice [46], the microstructural dependence of fracture energy (γ) comprehends the grain size (G), the composition, the porosity (P) and the combined effects of them.

Concerning the grain size effect, the crystalline structure of material is important when evaluating behavior between G and γ. Overall, the cubic materials present less variation of γ with G.

On the other hand, as shown in **Figure 12** for some noncubic ceramics, they present rising values of fracture energy (γ) until the maximum and, then, there is a decrease as the grain size (G) increases. This effect is attributed to the thermal expansion anisotropy, which occurs only in noncubic materials, but the intensity of it varies among materials [47].

Changes in the ceramic composition can also lead to a similar effect related to the grain size. These changes can be due to chemical composition or by introducing a more compliant grain boundary phase; both changes can modify the thermal expansion anisotropy affecting the fracture energy (γ) behavior of the material. There are several examples in the literature showing this behavior for Al_2O_3-ZrO_2 system, and SiC and Si_3N_4 with additions of oxides.

Although there are more limited data about the relation between fracture energy and porosity ($\gamma \times$ P) in comparison to fracture energy and grain size($\gamma \times$ G), some tendencies can be mentioned.

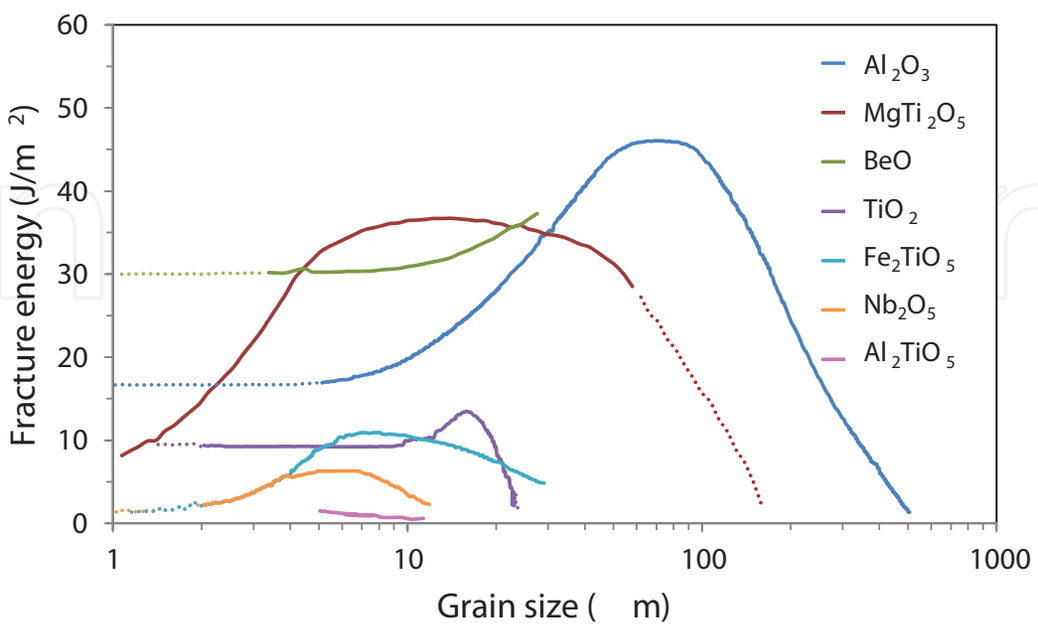

Figure 12. Fracture energy (γ) as a function of grain size (G) for noncubic oxide ceramics at 22°C [47].

At first, in single-phase ceramics with fine-to-medium-grain size, the fracture energy (γ) decreases as porosity (P) increases, following a similar tendency to the one found for mechanical strength (see **Figure 2**). Overall, this tendency has been shown in many advanced ceramics with porosity up to 50% [47].

Nevertheless, there are some works indicating the rate of fracture energy decrease can be reduced or even reversed [37, 47]. For instance, porous-fused SiO_2 (P~13–20%) provided fracture energy (γ) equal to or greater than the obtained value for dense SiO_2 glass.

Additional examples comprehend porous composite SiC-Al_2O_3-C (P~30–40%) and reaction sintered Si_3N_4 (P~45%). However, in all cases, the fracture energy (γ) decreased again at high porosity level (P) because the γ value goes to zero as P achieves 100%.

Considering there is not a consensus concerning the relation between fracture energy and porosity, we would like to propose a discussion about the influence of porosity on the fracture energy measurements of porous ceramics and, consequently, on their fracture toughness values.

Recently, Salvini et al.[43] have shown that fracture energy values for macroporous foamed Al_2O_3 can vary significantly depending on the test conditions. According to them, this is because of the following two factors: (1) the stress intensity factor at the notch tip may be decreased by the presence of surrounding pores (crack-tip blunting mechanism) as shown in **Figure 13** and (2) there is a strong interaction of cracks with the pores in the microstructure.

Although many researchers use a single test sample, Salvini et al. [48] carried out tests on separated notched macroporous samples for the two energy measurements γ_{eff} and γ_{WOF}. The

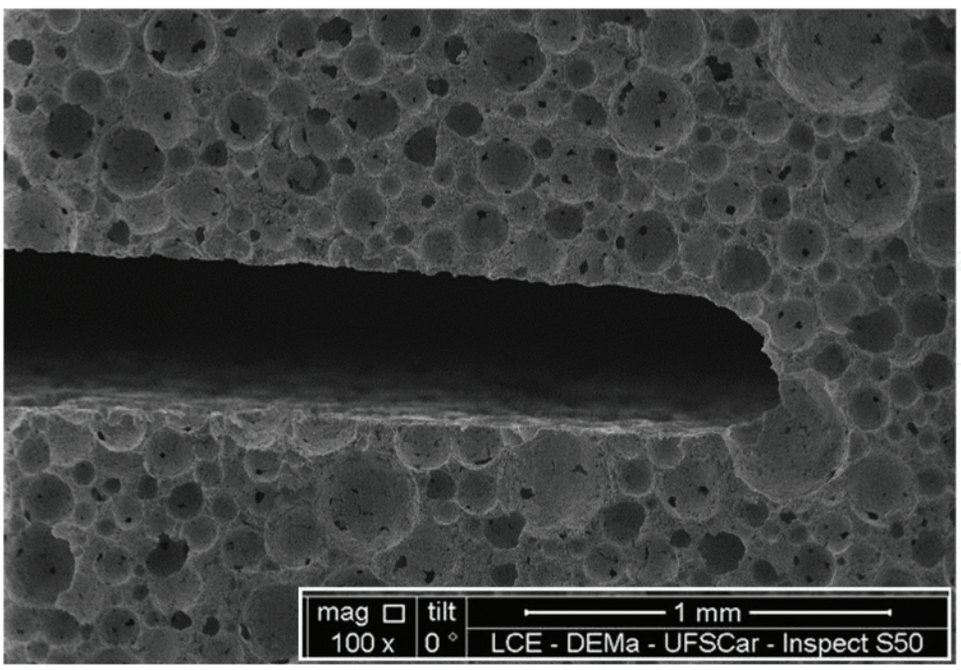

Figure 13. Macroporous foamed Al_2O_3 sample notched with a 300-μm thick diamond blade where the crack-tip blunting mechanism is shown [58].

γ_{eff} represents the fracture surface energy to initiate crack propagation, as proposed by Evans [49], whereas the total work-of-fracture γ_{WOF} expresses the energy to propagate a crack through the specimen thickness, as suggested by Nakayma [50]. A similar approach has been applied in evaluating fracture energy in materials with coarse microstructures, for example, in refractory ceramics [51, 52].

The fracture toughness (K_{IC}) was determined according to the ASTM E-399 at room temperature in a three-point bend test applying the equation:

$$K_{IC} = \frac{F \times S}{B \times W^{3/2}} \times f\left(\frac{a}{W}\right) \tag{5}$$

where F is the fracture load (N), S is the span (m), B is the specimen width, W is the specimen thickness, a corresponds to the crack size, and f (a/W) is obtained by the following expression:

$$f\left(\frac{a}{W}\right) = 3\sqrt{\frac{a}{W}} \times \frac{1.99 - \left(\frac{a}{W}\right) \times \left(1 - \frac{a}{W}\right)\left[2.15 - 3.93\frac{a}{W} + 2.7\left(\frac{a}{W}\right)^2\right]}{2\left(1 + 2\frac{a}{W}\right)\left(1 - \frac{a}{W}\right)^{3/2}} \tag{6}$$

The bar samples were center-notched to one-half of their thickness $(a/W \approx 0.5)$ with a 300-μm thick diamond blade for the K_{IC} measurements. All fracture energy tests were performed on a MTS 180 machine in three-point bending over a span of 125 mm. For K_{IC}, fracture surface energy (γ_{eff}) measurements were carried out at a stress loading rate of 1.5 kN/s.

This measured value of K_{IC} was then used to calculate the energy for crack initiation (γ_{eff}) by the expression:

$$K_{IC} = \left(2\gamma_{eff}E\right)^{1/2} \tag{7}$$

where E is Young's elastic modulus measured by a sonic technique in foamed Al_2O_3 bar samples (E = 18 GPa). Further details about this technique can be found in Ref. [53].

For the total work-of-fracture (γ_{WOF}) measurements, the foamed Al_2O_3 bar samples were also center-notched with a 300-μm thick diamond blade so that one-half of their thickness cross section remained. The samples were loaded in three-point bending at a crosshead speed of 0.001 mm/min to ensure stable crack growth (ASTM C1368–10). The total work-of-fracture (γ_{WOF}) values were then calculated by:

$$\gamma_{WOF} = \frac{\int F\,dx}{2\,A} \tag{8}$$

where $\int F\,dx$ represents the required work for new surfaces' generation and A is the projected area of the new fracture surfaces, as determined directly from the individual specimen notched areas.

Table 2 shows the obtained experimental results of the fracture energies (γ_{eff} and γ_{WOF}) and the fracture toughness (K_{IC}) for the foamed Al_2O_3.

Density, ρ (g/cm^3)	γ_{eff} (J/m^2)	γ_{WOF} (J/m^2)	K_{IC} (MPa.m$^{1/2}$)
0.86 ± 0.02	4.68 ± 0.5	15.81 ± 0.8	0.42 ± 0.03
0.87 ± 0.01	3.62 ± 0.3	14.46 ± 0.95	0.35 ± 0.05
0.90 ± 0.02	3.72 ± 0.6	15.39 ± 1.0	0.37 ± 0.02
0.92 ± 0.02	4.15 ± 0.8	12.27 ± 1.1	0.36 ± 0.02
0.94 ± 0.03	3.55 ± 0.35	13.32 ± 0.9	0.34 ± 0.09

Table 2 Results of fracture energies (γ_{eff} and γ_{WOF}) and the fracture toughness (K_{IC}) for macroporous foamed Al_2O_3 [58].

The K_{IC} values in **Table 2** were the expected ones for highly porous ceramics and they were compatible with data from the literature [24, 54, 55]. However, these results must be interpreted carefully, because of the crack-tip blunting mechanism due to the presence of surrounding pores (see **Figure 13**). This mechanism may decrease the stress intensity factor at the notch tip. Consequently, the crack propagation should not follow the required linear-elastic conditions for the fracture toughness measurement.

Based on that, we would like to raise the following issues: Does it make sense to measure the fracture toughness (K_{IC}) of porous ceramics knowing that the stress intensity factor at the notch tip is decreased by the crack-tip blunting? Or, instead of this, would the total work-of-fracture energy be a more realistic measure for these materials?

The results of total work-of-fracture energy (γ_{WOF}) presented in **Table 2** agree with the values obtained for Al_2O_3 produced using intermediate grain sizes (10–50 μm) [56].

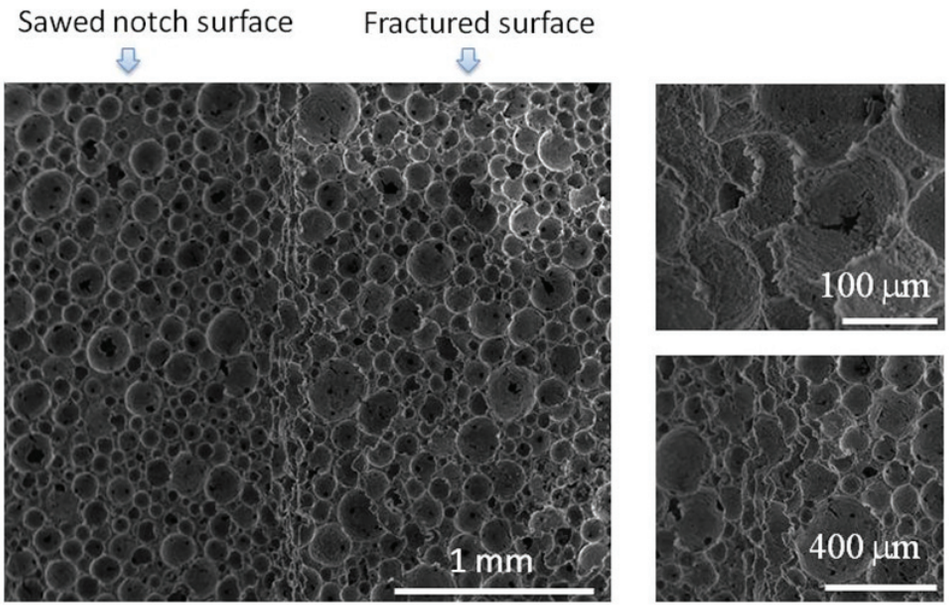

Figure 14. Fracture surface of macroporous foamed Al_2O_3 showing the characteristics of the fracture and notched surfaces [58].

Nevertheless, there is few data in the literature concerning fracture energies of porous ceramics. Kanhed et al. [57] found fracture toughness values in the range of 0.55–0.86 $MPa\ m^{1/2}$ for porous hydroxyapatite.

Considering the fracture surface microstructure of foamed Al_2O_3 presented in **Figure 14**, it seems that the fracture energy increase induced by porosity and the fracture energy reduction caused by decreased solid concentration are combined to describe the total work-of-fracture energy of material. However, more research on this topic is therefore recommended.

4. Elastic modulus behavior of porous ceramics

As well known, accurate elastic moduli are measured dynamically by measuring the frequency of natural vibrations of a beam, or by measuring the velocity of sound waves in the material. Both depend on $\sqrt{E/\rho}$, so if density (ρ) is known, E can be determined. These properties (ρ, E) reflect the mass of atoms, the way they are packed in material and the stiffness of the bonds that hold them together. For instance, **Table 3** presents the literature data of elastic modulus for several synthetic and natural porous brittle materials.

Considering that microscaled damage in ceramics can be caused in processing as well as during their application, a technique that detects the in situ microcracks evolution is important to estimate the life operation of them [65].

The *in situ* elastic modulus measurement as a function of temperature may identify the causes of microcracks in material, which is very helpful to adjust ceramic processing and design the material microstructure for an extended period of use.

Material	Porosity (%)	Elastic modulus (GPa)
Porous hydroxyapatite (HA) [5]	82–86	0.002–0.83
Cortical bone [5, 59, 60]	5–15	7–18
Cancellous bone [5, 59, 60]	~90	0.1–5
Cordierite diesel particulate filter (DPF) [54]	~50	12–13
Porous clay ceramics [55]	35–50	1–3
Silicon oxycarbide ceramic foams [24]	70–85	1–7
Porous SiC preforms [61]	30–65	30–120
Porous Si_3N_4 [62, 63]	35–55	45–105
Gelcasting Al_2O_3 foams [63]	60–85	10–65
Foamed Al_2O_3 [48]	76–80	15–18
SiC filters for metals [64]	85–92	2–3

Table 3. Elastic modulus values for porous and brittle materials.

In this context, this section is divided into two parts. In the first part, a review about theoretical models to describe the effect of porosity on the elastic modulus of porous ceramics is presented. Then, the second part presents and discusses the elastic modulus behavior as a function of temperature for the foamed Al_2O_3 ceramics.

Much research over the last decades was dedicated to understanding the influence of the porosity on the elastic modulus of ceramics. **Table 4** shows the most common theoretical models concerning the elastic modulus (E) and the porosity (P) correlations.

The Knudsen [66] and Rice [28] models fit well with real data of materials with porosity lower than 50%, as reported by Boccaccini et al. [67] and Ohji et al. [62, 63].

The model proposed by MacKenzie [68] and Kingery [69] is also defined for a lower level of closed pores.

Gibson and Ashby (GA) models [22, 23] indicated that the elastic modulus of a porous material depends only on its relative density and pore morphology.

Boccaccini model [67] introduced the *s* parameter to indicate the porosity geometry effect on the elastic modulus, that is, the pore shape and its orientation. However, it is valid only for low porosity level (P < 0.4) of closed pores.

In another work Boccaccini et al. [70] also included the topological parameters of highly porous microstructure to the model, besides the geometrical ones. Topological characterization comprehends the separation, the separated volume and the degree of contact and separation in two-phase microstructures. However, an issue that was addressed by the authors in this model is the necessity of a well-characterized porous structure of material, besides its porosity, to achieve rigorous verification of the model.

Model	Characteristics	
$E = E_0 e^{-bP}$ Refs. [28, 66]	Dependent on P and on extent of contact between solids	Valid for $P < 0.5$ and isotropic material
$E = E_0\left(1 - 1.9P + 0.9P^2\right), P \leq 0.5$ Refs. [67, 68]	Dependent on the closed pores' concentration	Valid for $P < 0.5$ and isotropic material
$E = C\,E_0\left(\frac{\rho}{\rho_s}\right)^n, C \approx 1\ and\ 1 < n < 2$ Refs. [22, 23]	Dependent on relative density and pore type	Valid for open porous and isotropic material
$E = E_0\left(1 - P^{2/3}\right)^s$ $s = 1.21\left(\frac{z}{x}\right)^{1/3}\left\{1 + \left[\left(\frac{z}{x}\right)^{-2} - 1\right]\right\}^{1/2}\cos^2\theta$ Ref. [67]	Dependent on P and on porosity geometry of closed pores	Valid for $P < 0.4$ and anisotropic material
$E = E_0\ \frac{(1-P)^2 R}{P+(1-P)R}$ $R = \frac{d_\beta}{d_\alpha}$, size ratio Ref. [69]	Dependent on P, on geometry and on topology of porosity	Valid for $R < 1$ and anisotropic material

Table 4 Summary of the elastic modulus (E) and porosity (P) models, where E_0 refers to the elastic modulus of solid material.

Overall, little research in the literature considers porous ceramics as anisotropic material in the evaluation of their elastic modulus behavior.

For instance, Rodrigues et al. [71] compared experimental data of the elastic moduli of Al_2O_3 foams (P: 60–90%) to several models proposed in the literature, as depicted in **Figure 15**. These authors considered the Al_2O_3 foams as isotropic material and, therefore, the experimental data fitted well with the MacKenzie [68] and Gibson and Ashby (GA) [22, 23] models.

This analysis, however, needs to be considered carefully because the foamed ceramics of high porosity (P > 60%) are usually anisotropic material and the mentioned models are valid only for homogeneous and isotropic ones.

Roy et al. [61], Wu et al. [59] and Lichtner [28] clearly showed that the extent of anisotropy, and its effect on the elastic modulus measurements, is strongly dependent on the porosity level, mainly for porosities higher than 40%, which is the case of the most foamed ceramics and natural porous materials.

Moving to the elastic modulus behavior at heating, Salvini et al. [48] evaluated the *in situ* elastic modulus behavior of foamed Al_2O_3 to identify the changes at the curing, drying and sintering stages of material.

The tests of elastic modulus were carried out in the range of temperature from 50 to 1400°C in air with heating and cooling rates of 2°C/min and a holding time of 4 h at 1400°C. After that, additional thermal cycles of elastic modulus measurements were carried out up to 1400°C.

Green bar samples (25 mm × 25 mm × 150 mm) of foamed Al_2O_3 containing 5 wt% of high alumina cement were considered for the *in situ* elastic modulus evaluation. The measurements

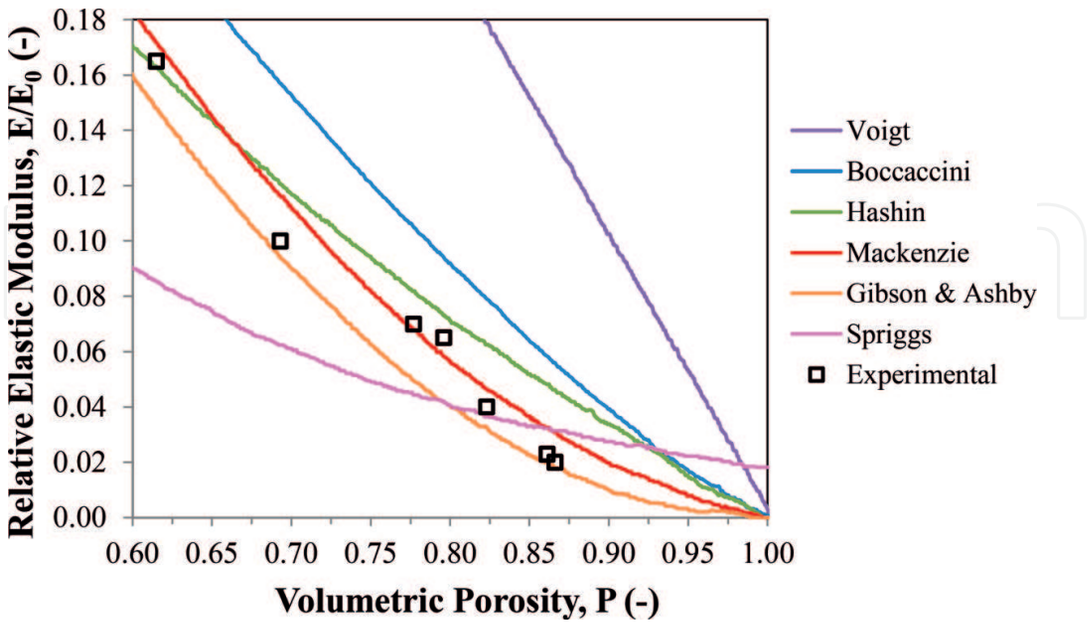

Figure 15. Theoretical models predicting the effect of porosity on the relative Young's modulus (continuous lines) and experimental data of gelcasting Al_2O_3 foams [71].

were carried out according to ASTM C1198–91 using the resonance bar technique (Scanelastic equipment, ATCP, Brazil).

Figure 16 depicts the in situ elastic modulus evolution (first and second cycles) up to 1400°C, in addition to results of the as-sintered foamed Al_2O_3 at 1500°C/4 h. **Table 5** presents the crystalline phase changes obtained by X-ray diffraction as a function of temperature for ceramic composition.

The foaming and casting processes of Al_2O_3 suspension were carried out at room temperature (~25°C). As reported by the literature [72], the main cement hydrate phase formed at room temperature is CAH_{10} ($CaO.Al_2O_3.10H_2O$). When the temperature increases, this phase partially dehydrates ~110°C into a mixture of gibbsite, AH_3 ($Al_2O_3.3H_2O$) and tricalcium aluminate hydrate, C_3AH_6 ($CaO.Al_2O_3.6H_2O$). This suggests that the drop of

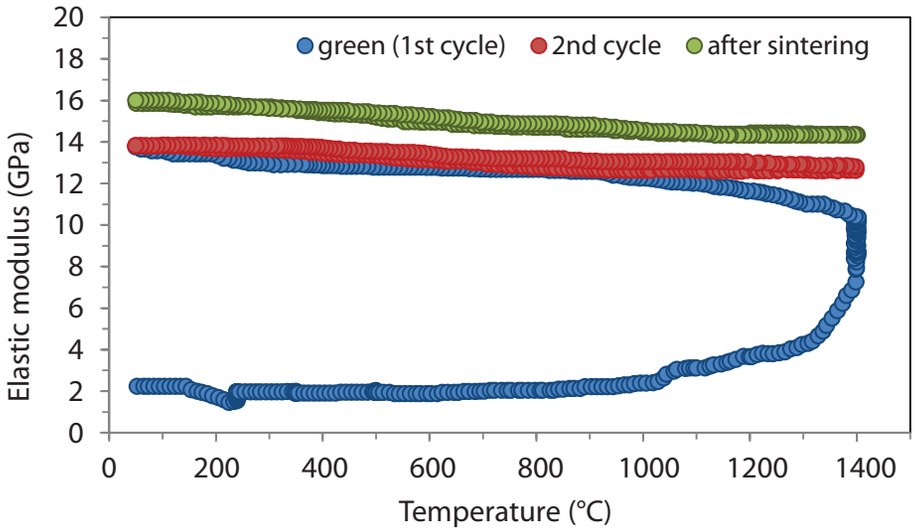

Figure 16. In situ elastic modulus of macroporous Al_2O_3: blue curve corresponds to the first cycle up to 1400°C of the green sample; the red curve is the measurement after the first cycle, and the green curve corresponds to the measurement after sintering up to 1500°C/4 h. The arrows indicate the discontinuities in the curve caused by decomposition or formation reactions of specific ceramic phases [48].

Crystalline phases	110°C	1000°C	1200°C	1400°C	1500°C
α-Al_2O_3	******	******	******	******	******
Al2O3.3H2O, AH3	**				
CaO. $Al_2O_3.6H_2O$, C_3AH_6	**				
$CaO.Al_2O_3$, CA		***	*		
$CaO.2Al_2O_3$, CA_2		*	***	****	*
$CaO.6Al_2O_3$, CA_6					***

Table 5 Phase changes obtained by X-ray diffraction in alumina composition containing 5 wt% of high alumina cement. The concentration of phases is qualitatively defined by the number of asterisks (*) displayed [48].

modulus curve observed in the initial stage of heating of the first cycle was caused by the conversion of $CAH_{10.}$

At higher temperatures, the discontinuities in the temperature range of 200–400°C were probably due to dehydration of the phases AH_3 ($Al_2O_3.3H_2O$) and C_3AH_6 ($CaO.Al_2O_3.6H_2O$), besides the decomposition of the organic additives (surfactants).

After dehydration, the elastic modulus remains stable at a low value until sintering starts at ~900°C. After 1100°C, the modulus increases rapidly due to sintering involving phase changes and formation of strong atomic bonds, which are characteristics of ceramic compositions.

At ~900°C, the CA ($CaO.Al_2O_3$) is the first crystalline phase formed, then it reacts with Al_2O_3 giving CA_2 ($CaO.2Al_2O_3$) at around 1100°C. The formation of CA_2 from CA and Al_2O_3 is expansive as a result of anisotropic growth of crystals [72].

At higher temperatures, the following two competitive phenomena occur: (1) expansion due to the formation of CA_2 phase and (2) shrinkage due to sintering of Al_2O_3 particles.

In the second cycle of measurement, no significant difference in the modulus curve was found in comparison with the first one.

In contrast, in case of sintering at 1500°C/4 h, the calcium hexa-aluminate CA_6 ($CaO.6Al_2O_3$) phase is additionally formed due to a reaction of CA_2 with Al_2O_3, which starts at ~1450°C. The formation of CA_6 is also expansive, leading to a superior elastic modulus of material.

Finally, when cooling the modulus curves remained stable without discontinuities, indicating an absence of microcracking of material.

These findings enhance the understanding not only about the role of specific additives (surfactants and inorganic binders) but also about the crystalline phase transformations and corresponding dimensional changes at sintering of macroporous ceramics. These results have important implications for developing porous ceramics with superior mechanical properties.

5. Summary

This chapter reviews the mechanical properties of porous ceramics with special interest on the mechanical strength, fracture toughness and elastic modulus of these materials.

One of the more significant findings to emerge from analysis of mechanical strength section is that, in addition to the porosity of porous ceramics, the number of connecting struts between the cells/pores in the microstructure plays a fundamental role in their mechanical strength behavior. Data from the literature support that once the connecting struts are lost in the porous structure, it is impossible to recover the original mechanical strength of it by merely increasing the struts thickness.

Regarding to fracture toughness of porous ceramics, two factors appear to control this property: the presence of surrounding pores at the crack front and the interaction of cracks with the pores in the microstructure.

Finally, the in situ hot elastic modulus analysis appears as an important method to better understand the processing steps as well as for predicting the life operation of this class of ceramic materials.

Author details

Vânia Regina Salvini[1]*, Victor C. Pandolfelli[2] and Dirceu Spinelli[3]

*Address all correspondence to: vr.salvini@gmail.com

1 College of Technology FATEC Sertãozinho, Sertãozinho, Brazil

2 Materials Engineering Department, Materials Microstructure Engineering Group GEMM, Federal University of São Carlos UFSCar, São Carlos, Brazil

3 Materials Engineering Department, EESC-USP São Carlos, São Carlos, Brazil

References

[1] Salvini VR, Innocentini MDM, Pandolfelli VC. Optimizing permeability, mechanical strength of ceramic foams. The American Ceramic Society Bulletin. 2000;**79**(5):49-54

[2] Sutton WH, Palmer JC, Morris JC. Development of ceramic foam materials for filtering high temperature alloys. AFS Transactions. 1985;**51**:339-346

[3] Salvini VR, Luz AP, Pandolfelli VC. High temperature Al_2O_3-CA_6 insulating foamed ceramics: Processing and properties. Interceram. 2012;**6**:335-339

[4] Sato M, Tomohide T, Kohji K, Akihiro S. Energy saving of slab reheating furnaces by improvements of refractories. In: Proceedings of the ACerS Unified International Technical Conference of Refractories (UNITCER´13); 10–13 September. Victoria Island, Canada: ACerS; 2013. pp. 333-338

[5] Rezwan K, Chen QZ, Blaker JJ, Boccaccini AR. Biodegradable and bioactive porous polymer/inorganic composite scaffolds for bone tissue engineering. Biomaterials. 2006;**27**:3413-3431. DOI: 10.1016/j.biomaterials.2006.01.039

[6] Jones JR, Hench LL. Regeneration of trabecular bone using porous ceramics. Current Opinion in Solid State and Materials Science. 2003;**7**:301-307. DOI: 10.1016/j.cossms.2003.09.012

[7] Teraoka K, Kato T, Hattori K, Ohgushi H. Evaluation of the capacity of mosaic-like porous ceramics with designed pores to support osteoconduction. Journal of Biomedical Materials Research Part A. 2013;**101**(12):3571-3579. DOI: 10.1002/jbm.a.34663

[8] Oyanedel-Craver VA, Smith JA. Sustainable colloidal-Silver-impregnated ceramic filter for point-of-use water treatment. Environmental Science & Technology. 2008;**42**(3):927-933. DOI: 10.1021/es071268u

[9] Pia G, Canedi L, Ionta M, Sanna U. On the elastic deformation properties of porous ceramic materials obtained by pore-forming agent method. Ceramics International. 2015; **41**:11097-11105. DOI: 10.1016/j.ceramint.2015.05.057

[10] Yang C, Zhang G, Xu N, Shi J. Preparation and application in oil-water separation of ZrO_2/α-Al_2O_3 MF membrane. Journal of Membrane Science. 1998;**142**:235-243. DOI: 10.1016/S0376-7388(97)00336-0

[11] Arcos D, Vallet-Regí M. Bioceramics for drug delivery. Acta Materialia. 2013;**61**:890-911. DOI: 10.1016/j.actamat.2012.10.039

[12] Treccani L, Klein T Y, Meder F, Pardun K, Rezwan K. Functionalized ceramics for biomedical, biotechnological and environmental applications. Acta Biomaterialia. 2013;**9**(7):7115-7150. DOI: 10.1016/j.actbio.2013.03.036

[13] Warren SC, Perkins MR, Adams AM, Kamperman M, Burns AA, Arora H, Herz E, Suteewong T, Sai H, Li Z, Zwanziger JW, Graetzel M, Disalvo FJ, Wiesner U. A silica sol-gel design strategy for nanostructured metallic materials. Nature Materials. 2012;**11**:460-467. DOI: 10.1038/nmat3274

[14] Suzuki Y, Hwang H J, Kondo N, Ohji T, In situ processing of a porous calcium Zirconate/Magnesia composite with Platinum nanodispersion and its influence on nitride oxide decomposition. Journal of the American Ceramic Society. 2001;**84**(11):2713-2715. DOI: 10.1111/j.1151-2916.2001.tb01079.x

[15] Bradt RC. Fracture mechanics of brittle ceramics – 30 years of progress. In: Salem A, Quinn GD, Jenkins MG, editors. Fracture Resistance of Monolithic and Composite Brittle Materials. West Conshohocken, PA: ASTM; 2002. pp. 3–13

[16] Zhang D, Zhang W, Gu J, Zhu S, Su H, Liu Q, Fan T, Ding J, Guo Q. Bio-inspired functional materials templated from nature materials. KONA Powder and Particle Journal. 2010;**28**:116-130. DOI: 10.14356/kona.2010011

[17] Ritchie RO. Armoured oyster shells. Nature Materials. 2014;**13**:435-437. DOI: 10.1038/nmat3956

[18] Meyers MA, Mckittrick J, Chen P-Y. Structural biological materials: Critical mechanics-materials connections. Science. 2013;**339**:773-779. DOI: 10.1126/science.1220854

[19] Fukasawa T, Ando M, Ohji T, Kanza S. Synthesis of porous ceramics with complex pore structure by freeze-dry processing. Journal of the American Ceramic Society.2001;**84**(1):230-232. DOI: 10.1111/j.1151-2916.2001.tb00638.x

[20] Launey ME, Munch E, Alsem DH, Barth HB, Saiz E, Tomsia AP, Ritchie RO. Designing highly toughened hybrid composites through nature-inspired hierarchical complexity. Acta Materialia. 2009;**57**:2919-2932. DOI: 10.1016/j.actamat.2009.03.003

[21] Genet M, Couégnat G, Tomsia AP, Ritchie RO. Scaling strength distributions in quasi-brittle materials from micro- to macro-scales: A computational approach to modeling nature-inspired structural ceramics. Journal of Mechanics and Physics of Solids. 2014;**68**:93-106. DOI: 10.1016/j.jmps.2014.03.011

[22] Ashby MF. The mechanical properties of cellular solids. Metallurgical Transactions A. 1983;**14**(9):1755-1769. DOI: https://doi.org/10.1007/BF02645546

[23] Gibson LJ, Ashby MF. Cellular solids – Structure and properties. 2nd ed. Cambridge: Cambridge University Press; 1999. ISBN-13: 978-0521499118

[24] Colombo P, Hellmann JR, Shelleman DL. Mechanical properties of silicon oxycarbide ceramic foams. Journal of the American Ceramic Society. 2001;**84**(10):2245-2251. DOI: 10.1111/j.1151-2916.2001.tb00996.x

[25] Seeber BSM, Gonzenbach UT, Gauckler LJ. Mechanical properties of highly porous alumina foams. Journal of Materials Research. 2013;**28**(17):2281-2287. DOI: 10.1557/jmr.2013.102

[26] Brezny R, Green DJ. The effect of cell-size on the mechanical behavior of cellular materials. Acta Metallurgica et Materialia. 1990;**38**(12):2517-2526. DOI: 10.1016/0956-7151(90)90263-G

[27] Salvini VR, Spinelli D, Pandolfelli VC. Mechanical behavior of foamed insulating ceramics. In: Ohji T, Matyás J, Manjooran NV, Pickrell G, Jitianu A, editors. Advances in Materials Science for Environmental and Energy Technologies III. New Jersey, USA: John Wiley & Sons; 2014. pp. 89-99. ISBN: 978-1-118-99668-3

[28] Lichtner A, Roussel D, Jauffres D, Martin CL, Bordia RK. Effect of macropore anisotropy on the mechanical response of hierarchically porous ceramics. Journal of the American Ceramic Society. 2016;**99**(3):979-987. DOI: 10.1111/jace.14004

[29] Brezny R, Green DJ, Dam CQ. Evaluation of strut strength in open-cell ceramics. Journal of the American Ceramic Society.1989;**72**(6):885-889. DOI: 10.1111/j.1151-2916.1989.tb06239.x

[30] Rice RW. Evaluation and extension of physical property-porosity models based on minimum solid area. Journal of Materials Science. 1996;**31**:102-118. DOI: 10.1007/BF00355133

[31] Bruno G, Kachanov M. Microstructure-property connections for porous ceramics: The possibilities offered by micromechanics. Journal of the American Ceramic Society. 2016;**99**(12):3829-3852. DOI: 10.1111/jace.14624

[32] Zheng M, Zheng X, Luo ZJ. Fracture strength of brittle porous materials. International Journal of Fracture. 1992;**58**:51-55. DOI: 10.1007/BF00015623

[33] Berek H, Halkova J, Aneziris CG. Characterization of cellular ceramics and MMC by in situ computed tomography. In: Presentation at the International Conference on Modern Materials and Technologies (13th CIMTEC), 8–13 June, Montecatini Therme, Italy: ECerS. 2014

[34] Petit C, Meille S, Maire E, Tadier S, Adrien J. Mechanical behavior of β-TCP ceramic with a random porosity: Study of the fracture path with X-ray tomography. Journal of the European Ceramic Society. 2016;**36**:3225-3233. DOI: 10.1016/j.jeurceramsoc.2016.05.001

[35] Cui Z, Huang Y, Liu H. Predicting the mechanical properties of brittle porous materials with various porosity and pore sizes. Journal of the Mechanical Behavior of Biomedical Materials. 2017;**71**:10-22. DOI: 10.1016/j.jmbbm.2017.02.014

[36] Morgan JS, Wood JL, Bradt RC. Cell size effects on the strength of foamed glass. Materials Science and Engineering. 1981;**47**:37-42. DOI: 10.1016/0025-5416(81)90038-0

[37] Deng Z-Y, She J, Langaki Y, Yang J-F, Ohji T, Tanaka Y. Reinforcement by crack-tip blunting in porous ceramics. Journal of the European Ceramic Society. 2004;**24**:2055-2059. DOI: 10.1016/S0955-2219(03)00365-0

[38] Peterson RE. Stress Concentration Design Factors. New York: John Wiley Inc.; 1953

[39] Rice RW. Limitations of pore-size concentrations on the mechanical properties of porous materials. Journal of Materials Science. 1997;**32**:4731-4736. DOI: 10.1023/A:101867471

[40] Morgan EL, Bouxsein ML. Biomechanics of bone and age-related fractures. In: Bilezikian JP, Raisz LG, Martin TJ, editors. Principles of Bone Biology. Vol. I. 3rd ed. Academic Press; 2008. pp. 29-51. ISBN: 0-12-098653-1

[41] Silva MJ, Gibson LJ. Modeling the mechanical behavior of the vertebral trabecular bone: Effects of age-related changes in microstructure. Bone. 1997;**21**(2):191-199. DOI: 10.1016/S8756-3282(97)00100-2

[42] Guo XE, Kim CH. Mechanical consequence of trabecular bone loss and its treatment: A three-dimensional model simulation. Bone. 2002;**30**(2):404-411. DOI: 10.1016/S8756-3282(01)00673-1

[43] Salvini VR. Processing and evaluation of fluid dynamic and thermomechanical properties of ceramic filters in the Al_2O_3-SiC system [thesis]. São Carlos: Federal University of São Carlos; 2000

[44] Ritchie RO. The conflicts between strength and toughness. Nature Materials. 2011;**10**:817-822. DOI: 10.1038/nmat3115

[45] Ashby MA, Sherliff H, Cebon D. Materials Engineering, Science, Processing and Design. 1st ed. Burlington, UK: Butterwoth-Heinemann; 2007. pp. 164-181

[46] Rice RW. Test-microstructural dependence of fracture energy measurements in ceramics in Fracture Mechanics for Ceramics. In: Freiman SW, Fuller Jr ER, editors. Rocks and Concrete. West Conshohocken: ASTM; 1982

[47] Rice RW. Grain size and porosity dependence of ceramic fracture energy and toughness at 22°C. Journal of Materials Science. 1996;**31**:1969-1983

[48] Salvini VR, Lasso PRO, Luz AP, Pandolfelli VC. Nontoxic processing of reliable macroporous ceramics. International Journal of Applied Ceramic Technology. 2016;**13**(3):522-531. DOI: 10.1111/ijac.12521

[49] Evans AG. Energies for crack propagation in polycrystalline MgO. Philosophical Magazine. 1970;**22**(178):841-852. DOI: 10.1080/14786437008220952

[50] Nakayama J, Abe H, Bradt RC. Crack stability in the work-of-fracture test: Refractory applications. Journal of the American Ceramic Society. 1981;**64**(11):671-675. DOI: 10.1111/j.1151-2916.1981.tb15868.x

[51] Sakai M, Ichikawa H. Work-of-fracture of brittle materials with microcracking and crack bridging. International Journal of Fracture. 1992;**55**:65-79

[52] Salvini VR, Pandolfelli VC, Bradt RC. Extension of Hasselman's thermal shock theory for crack/microstructure interactions in refractories. Ceramics International. 2012;**38**:5369-5375. DOI: 10.1016/j.ceramint.2012.03.046

[53] Pickett G. Equations for computing elastic constants from flexural and torsional resonat frequencies of vibration of prisms and cylinders. In: Proceedings of the Portland Cement Association ASTM. 1945;**45**:846-865

[54] Shyam A, Lara-Curzio E, Watkins TR, Parten RJ. Mechanical characterization of diesel particulate filter substrates. Journal of the American Ceramic Society. 2008;**91**(6):1995-2001. DOI: 10.1111/j.1551-2916.2008.02381.x

[55] Yakub I, Du J, Soboyejo WO. Mechanical properties, modeling and design of porous clay ceramics. Materials Science & Engineering A. 2012;**558**:21-29. DOI: 10.1016/j.msea.2012.07.038

[56] Doerre E, Huebner H, Alumina: Processing, Properties, and Applications. 1st ed. Berlin: Springer-Verlag Press; 1984. 329 p. ISBN: 3-540-13576-6

[57] Kanhed S, Awasthi S, Goel S, Pandey A, Sharma R, Upadhyaya A, Balani K. Porosity distribution affecting mechanical and biological behavior of the hydroxyapatite bioceramic composite. Ceramics International 2017,**43**:10442–10449. DOI:10.1016/j.ceramint.2017.05.083

[58] Salvini VR, Spinelli D, Pandolfelli VC. Thermomechanical properties of macro-porous alumina. In: Presentation at the ECerS International Conference on Modern Materials and Technologies (13th CIMTEC), 8–13 June, Montecatini Therme, Italy: ECerS; 2014

[59] Wu S, Liu X, Yeung KWK, Liu C, Yang X. Biomimetic porous scaffolds for bone tissue engineering. Materials Science and Engineering R. 2014;**80**:1-36. DOI: 10.1016/j.mser.2014.04.001

[60] Dong XN, Guo XE. The dependence of transversely isotropic elasticity of human femoral cortical bone on porosity. Journal of Biomechanics. 2004;**37**:1281-1287. DOI: 10.1016/j.jbiomech.2003.12.011

[61] Roy S, Schell K G, Bucharsky E C, Weidenamann K A, Wanner A, Hoffman M J. Characterization of elastic properties in porous SiC performs fabricated using polymer waxes as pore formers. Journal of the American Ceramic Society. 2013;**96**(7):2269-2275. DOI: 10.1111/jace.12341

[62] Yang J-F, Ohji T, Kanzaki S, Díaz A, Hampshire S. Microstructure and mechanical properties of silicon nitride ceramics with controlled porosity. Journal of the American Ceramic Society. 2002;**85**(6):1512-1516. DOI: 10.1111/j.1151-2916.2002.tb00305.x

[63] Ohji T. Microstructural design and mechanical properties of porous silicon nitride ceramics. Materials Science and Engineering A. 2008;**498**:5-11. DOI: 10.1016/j.msea.2007.09.104

[64] ERG Materials and Aerospace Corporation. 2017. Available from http://www.ergaerospace.com/SiC-properties.htm [Accessed: 2017-11-01]

[65] Yonezy A, Chen X. Micro-scale damage characterization in porous ceramics by an acoustic emission technique. Ceramics International. 2014;**40**(7):9859-9866. DOI: 10.1016/j.ceramint.2014.02.079

[66] Knudsen FP. Dependence of mechanical strength of brittle polycrystalline specimens on porosity and grin size. Journal of the American Ceramic Society. 1959;**42**(8):376-387. DOI: 10.1111/j.1151-2916.1959.tb13596.x

[67] Boccaccini AR, Fan Z. A new approach for the Young's modulus – Porosity correlation of ceramic materials. Ceramics International. 1997;**23**:239-245. DOI: 10.1016/S0272-8842(96)00033-8

[68] Mackenzie JK. The elastic constants of a solid containing spherical holes. Proceedings of Physical Society B. 1950;**63**(1):2-11. DOI: 10.1088/0370-1301/63/1/302

[69] Kingery WD, Bowen HK, Uhlmann DR. Introduction to Ceramics. 2nd ed. USA: John Wiley & Sons; 1976. pp. 773-781. ISBN: 0-471-47860-1

[70] Boccaccini DN, Boccaccini AR. Effect of pore shape on the ultrasonic velocity-porosity correlation in sintered materials. Journal of Materials Science Letters.1997;**16**:623-625. DOI: 10.1023/A:101850703

[71] Rodrigues JA, Ortega FS, Paiva AEM, Villaboim ELG, Pandolfelli VC. The relation between porosity and elastic moduli of gelcast ceramic foams. Cerâmica. 2004;**50**:209-216. DOI: 10.1590/S0366-69132004000300007

[72] Nonmet E, Lequeux N, Boch P. Elastic properties of high alumina cement castables from room temperature to 1600°C. Journal of the European Ceramic Society.1999;**19**:1575-1583

IntechOpen